Intraplacental injection of human iPSC-derived PDX1+ pancreatic progenitors prolongs Pdx1-deficient mice survival

Arata Wakimoto[1,2,†], Zeynab Javanfekr Shahri[1,3,†], Hyojung Jeon[1,4], Takuto Hayashi[5], Ching-Wei Liao[1,3], Natalia Gogoleva[1,3], Fabian Suchy[6], Atsushi Noda[1], Yuri An[7], Hiromitsu Nakauchi[6,8], Yohei Hayashi[7, 10]* ,Michito Hamada[1,9,11]*, Satoru Takahashi[1,9]*

1. Department of Anatomy and Embryology, Faculty of Medicine, University of Tsukuba, 1‐1‐1, Tennodai, Tsukuba, Ibaraki 305‐8575, Japan.
2. Department of Obstetrics and Gynecology, School of Medicine, University of Washington, Seattle, WA 98109, USA
3. Ph.D. Program in Human Biology, School of Integrative and Global Majors, University of Tsukuba, 1‐1‐1, Tennodai, Tsukuba, Ibaraki 305–8575, Japan.
4. Division of Cell Regulation, Center of Experimental Medicine and Systems Biology, The Institute of Medical Science, The University of Tokyo, 4-6-1 Shirokanedai, Minato-ku, Tokyo 108-8639, Japan.
5. Univ Paris Est Creteil, INSERM, IMRB, F-94010 Creteil, France.
6. Institute for Stem Cell Biology and Regenerative Medicine, Stanford University School of Medicine, Stanford, CA 94305, USA.
7. iPS Cell Advanced Characterization and Development Team, BioResource Research Center, RIKEN, 3-1-1 Koyadai, Tsukuba, Ibaraki 305-0074, Japan.
8. Stem Cell Therapy Laboratory, Advanced Research Institute, Tokyo Medical and Dental University (TMDU), Bunkyo-ku, Tokyo 113-8510, Japan.
9. Laboratory Animal Resource Center, Faculty of Medicine, University of Tsukuba, 1‐1‐1, Tennodai, Tsukuba, Ibaraki 305‐8575, Japan.
10. CiRA Foundation, Nakanoshima Qross 7F, 4-3-51 Nakanoshima, Kita-ku, Osaka, 530-0005, Japan
11. Center for Medical Sciences, Ibaraki Prefectural University of Health Sciences, 4669-2 Ami, Inashiki-gun, Ami-machi, Ibaraki, Japan

†. These authors contributed equally to this work and may list their name first in their curriculum vitae.

*Correspondence;
yohei.hayashi@riken.jp (Y.H.), hamamichi@md.tsukuba.ac.jp (M.H.),
satoruta@md.tsukuba.ac.jp (S.T.)

Summary

Interspecies chimeras comprising human tissues have potential for use in disease modeling and regenerative medicine. Here, we successfully transplanted human induced pluripotent stem cell (iPSC)-derived PDX1+ pancreatic progenitor cells into *Pdx1*-deficient mouse embryos via intraplacental injection. The engrafted human cells predominantly localized to the duodenum, produced insulin, and extended the lifespan of *Pdx1*$^{-/-}$ mice by up to 10 days after birth. Transcriptomic analyses confirmed human pancreatic gene expression in human cells engrafted into the mouse duodenum. Our findings demonstrated the feasibility of generating interspecies chimeras with functional human pancreatic cells through *in utero* transplantation of lineage-committed progenitors. This approach circumvents developmental barriers while minimizing ethical concerns associated with PSCs. However, the incomplete rescue of the *Pdx1*$^{-/-}$ phenotype highlights the need for further research to enhance human cell engraftment and tissue integration. Overall, this study provides a foundation for developing human-animal chimera models for studying human development and regenerative therapies.

Introduction

Interspecies chimeras with human tissues represent a promising approach for developing human disease models and generating organs for transplantation. Successful intraspecies (mouse-mouse) (Hamanaka et al., 2018) and interspecies (mouse-rat) (Goto et al., 2019; Kobayashi et al., 2021, 2010; Wu et al., 2017) chimeras have been established through blastocyst complementation. However, integrating functional human tissues into animal models has proven challenging (Hu et al., 2020; Maeng et al., 2021; Masaki et al., 2015; Wang et al., 2024).

An alternative approach for generating chimeric animals is to inject tissue stem/progenitor cells into a developing embryo using *in utero* injections (Cohen et al., 2020; Fleischman and Mintz, 1979; Fujiki et al., 2003; Jeon et al., 2021). Previous studies using neural crest cells successfully engrafted human cells into mouse embryos (Cohen et al., 2020, 2016). Utilizing lineage-committed cells minimizes the likelihood of donor cell differentiation for unintended purposes such as germline transmission and carcinogenesis (Crane et al., 2019; Wu et al., 2016).

Human pancreatic xenograft models are generated using newborn and adult NSG mice (Augsornworawat et al., 2020; Ma et al., 2018). These models have provided valuable insights into the functionality of human induced pluripotent stem cell (iPSC)-derived pancreatic cells *in vivo*. However, successful transplantation of human pancreatic

progenitors into mouse embryos has not yet been accomplished because of the low survival rate of *in utero* injection systems.

Previously, we developed an intraplacental injection method to deliver cells (Jeon et al., 2021) and virus vectors (Gogoleva et al., 2023) into mouse post-implantation embryos through the placenta. This technique offers higher embryonic survival rates (>80%) compared to direct *in utero* injection methods because it avoids direct embryonic penetration.

Along with the placental connection established at E9.5, the initial indication of pancreas formation occurs as the dorsal endodermal epithelium thickens just below the stomach (Puri and Hebrok, 2007). All known pancreatic cell lineages originate from a small cluster of precursor cells within the foregut endoderm as defined by the expression of pancreatic and duodenal homeobox 1 (*Pdx1*) (Byrnes et al., 2018). *Pdx1* is recognized as a master regulator of pancreatic development, and its deficiency results in a lack of the whole pancreas and postnatal lethality within a day (Offield et al., 1996).

Various methods exist for differentiating iPSCs into pancreatic cell types, especially pancreatic β cells (Liu et al., 2014; Loh et al., 2014; Ma et al., 2018; Pagliuca et al., 2014; Rezania et al., 2014; Shahjalal et al., 2014). Most differentiation protocols follow a stepwise approach involving the progression of PSCs to definitive endoderm, pancreatic progenitors, and finally, functional pancreatic β cells.

Therefore, we hypothesized that introducing human iPSC-derived PDX1+ pancreatic cells into *Pdx1*-deficient mouse embryos would enable the derivation of human pancreatic tissue by occupying this vacant developmental niche. In this study, we investigated a method to generate a mouse model with human pancreatic tissue by transplanting iPSC-derived human PDX1-positive cells into *Pdx1*$^{-/-}$ mice lacking a pancreas. The resulting human-mouse chimera exhibited prolonged survival compared with that of uninjected *Pdx1*$^{-/-}$ mice. The engrafted donor-derived cells were capable of secreting human insulin. Notably, the injected human cells were primarily engrafted ectopically, predominantly in the duodenum. Our findings suggest that the *in utero* transplantation of lineage-committed human cells can give rise to interspecific chimeras with functional human-derived cells.

Results

Establishment and characterization of engineered human iPSC lines

To conduct the intraplacental injection of human PDX1-expressing cells into *Pdx1*$^{-/-}$ mouse embryos, we first established two novel human iPSC lines with different tracking capabilities using CRISPR-mediated genome editing. The PDX1-P2A-tdTomato reporter line was generated by inserting a P2A-tdTomato cassette at the endogenous *PDX1* locus, enabling direct visualization of PDX1 expression during differentiation. The EEF1A1-iRFP670 line was created by integrating near-infrared fluorescent protein iRFP670 under the constitutive EEF1A1 promoter for robust cell tracking after injection. Both lines underwent characterization to confirm their pluripotent properties and differentiation potential. Immunostaining revealed robust expression of core pluripotency markers OCT3/4 and NANOG in undifferentiated colonies of both PDX1-tdTomato and EEF1A1-iRFP670 lines (Figure S1A, C). To assess differentiation potential, we performed embryoid body formation assays followed by immunostaining for lineage-specific markers. Both lines successfully differentiated into all three germ layers, as evidenced by expression of ectoderm markers (PAX6, TUJ1), mesoderm markers (HAND1, SMA), and endoderm markers (SOX17, AFP) (Figure S1B, D). These results confirmed that our newly established lines retained the fundamental pluripotent characteristics for subsequent pancreatic differentiation studies.

Pancreatic progenitor differentiation protocol optimization and validation

We adapted established protocols (Pagliuca et al., 2014; Rezania et al., 2014) for stepwise pancreatic differentiation, involving initial definitive endoderm induction with Activin A and CHIR99021, followed by pancreatic specification using retinoic acid, cyclopamine-KAAD, SB431542, and DMH-1 (Figure 1A). Using the PDX1-tdTomato reporter line, we confirmed 66.3 ± 7.4% colocalization between endogenous PDX1 protein and tdTomato expression at day 13 (Figure 1B). Flow cytometric analysis revealed that approximately 90% of viable cells expressed PDX1-tdTomato at day 13 (Figure 1C). We monitored the expression of key developmental markers by reverse transcription-quantitative PCR (RT-qPCR). From days 3 to 5, the definitive endoderm (DE) marker *SOX17* was upregulated (log2 fold change = 13). Subsequently, the pancreatic progenitor (PP) marker *PDX1* expression increased significantly (log2 fold change = 7), followed by expression of *NKX6-1* (log2 fold change = 4) by day 13 (Figure 1D). We validated our protocol using additional genetically independent human iPSC lines, WTC11 (GM25256, Coriell Institute), and NB1RGB (HPS5067, RIKEN Cell Bank). RT-qPCR analysis revealed consistent temporal dynamics of *PDX1*, *SOX17*, *HNF6*, *NANOG* across all three lines throughout the differentiation (Figure S2A-B). PDX1

immunostaining at day 13 showed PDX1-positive cells for the three lines (Figure S2C). These results established robust pancreatic progenitor differentiation across genetically distinct backgrounds. Furthermore, we performed flow cytometric analysis to assess differentiation efficiency. On day 6, definitive endoderm formation was confirmed by CXCR4 and CD117 across the three lines (Figure S3). By day 13, pancreatic progenitor specification was assessed through expression of NKX6-1, revealing 71.38% of cells were NKX6-1 positive (Figure S4). These analyses provided validation of efficient progression through definitive endoderm to pancreatic progenitor stages.

For detailed transcriptomic profiling and subsequent injection experiments, we used the EEF1A1-iRFP670 line. Although iRFP670 expression intensity decreased approximately 10-fold after pancreatic differentiation (Figure S1E), the signal remained robust enough for cell tracking in subsequent transplantation experiments. RNA sequencing (RNA-seq) was performed to further characterize the differentiated cells. A total of 11,747 differentially expressed genes (DEGs; false discovery rate [FDR] < 0.01) were identified, and principal component analysis (PCA) showed that the gene expression profiles were completely separated before and after differentiation (Figure S5A). Genes associated with pancreatic development were upregulated in differentiated cells (Figure 1E and S5B), whereas the pluripotency markers *NANOG*, *SOX2*, and *POU5F1* were significantly downregulated (Figure 1E). Conversely, the pancreatic progenitor signature genes *PDX1*, *SOX9*, *HNF1B*, *NKX6-1*, *FOXA2*, and *HOXB4* were significantly upregulated (Figure 1E, 1F, and S5B). However, the pancreatic endocrine progenitor genes *NEUROD1* was not upregulated (Figure S5C). Moreover, the pancreatic endocrine effector genes *INS*, *GCG*, *PPY*, and *SST* were not expressed (Figure 1F, Figure S5C). To investigate the differentiation potential of the pancreatic progenitors, we extended our culture protocol using a three-dimensional organoid system supplemented with betacellulin, exendin-4, and T3. After two additional weeks of culture, immunostaining revealed the presence of insulin-positive and glucagon-positive cells in organoids derived from all three cell lines (Figure S6), confirming that our PDX1-positive cells retained the capacity to further differentiate into pancreatic endocrine cells.

Taken together, these results demonstrated successful generation of PDX1-expressing pancreatic progenitor cells from multiple human iPSC lines with consistent efficiency and confirmed potential for endocrine differentiation. For subsequent injection experiments, we focused exclusively on the EEF1A1-iRFP670 line due to its superior cell tracking capabilities.

Intraplacental injection of human PDX1-positive cells did not inhibit embryonic development at low concentrations

To set the cell number for injection, we first intraplacentally injected human pancreatic cells at various concentrations into wild-type (WT) embryos (Figure 1G, H, Table S1) at E10.5. EEF1A-iRFP670 cells were differentiated into pancreatic cells after 13 days of differentiation culture. On day 3, we mated the *Pdx1*$^{+/-}$ mice to obtain E10.5 embryos on day 13 of culture (Figure 1G). The number of embryos was counted after injection. After injection, we waited for birth and counted the number of newborns to calculate the birth rate. The birth rate after injection was significantly lower (37, 37, 18, and 37%) at high concentrations (2×10^5 to 2.5×10^4 per embryo). On the other hand, low concentrations (1×10^4 and 5×10^3 per embryo) displayed birth rates comparable to that of the phosphate-buffered saline (PBS) injection control (>80%) (Figure 1H, Table S1). Frequent embryonic resorption was observed in mothers with low birth rates. Therefore, we set the concentration of cells at 1×10^4 per embryo in all subsequent experiments.

Human pancreatic cells extend the lifespan of *Pdx1*$^{-/-}$ mice

Next, human pancreatic cells were intraplacentally injected into E9.5 or E10.5 embryos obtained from *Pdx1*$^{+/-}$ mouse matings (Figure 2A). We confirmed that *Pdx1*$^{-/-}$ mice were born according to the Mendelian rule (Table S2). Uninjected *Pdx1*$^{-/-}$ newborns died a day after birth, as previously reported (Offield et al., 1996). On the other hand, human pancreatic cell-injected *Pdx1*$^{-/-}$ newborns survived up to 10 days, and their lifespans were significantly longer than those of uninjected mice ($p = 0.0013$ in the log-rank test) (Figure 2B). Thus, *Pdx1*$^{-/-}$ mice survived likely due to the contribution of human pancreatic cells. In our gross observations, the long-surviving *Pdx1*$^{-/-}$ mice appeared small and thin compared with their WT and *Pdx1*$^{+/-}$ littermates, indicating that the cells could not compensate for their growth abnormality (Figure 2C, D). In addition, pancreatic structures were not observed even in long-surviving *Pdx1*$^{-/-}$ (Figure 2E).

Therefore, although it did not correct the developmental abnormalities associated with their genotype, human pancreatic cell injection into *Pdx1*$^{-/-}$ mice extended their lifespan.

Human insulin production was detected in injected *Pdx1*$^{-/-}$ mice

Given that *Pdx1*$^{-/-}$ mice lack endogenous pancreatic β-cells and cannot produce insulin, we monitored blood glucose levels daily to assess potential functional human cell engraftment. Of the six *Pdx1*$^{-/-}$ mice injected at E9.5, two mice showed increased blood glucose levels to 350 mg/dL on the fourth day of life, which decreased to below the detection limit (20 mg/dL)

by the sixth day (Figure 2F). The other two did not show an increase in blood glucose and died on the third day of life. In contrast, mice injected at E10.5 showed no detectable glucose elevation throughout their survival period (Figure 2F). WT and *Pdx1*$^{+/-}$ littermates maintained stable glucose levels around 100 mg/dL regardless of injection timing (Figure 2F). Based on these observations, subsequent experiments were performed using E9.5 injection timing.

To assess human insulin production, human C-peptide in *Pdx1*$^{-/-}$ mouse serum was quantified using enzyme-linked immunosorbent assay (ELISA). Human C-peptide levels were significantly elevated at postnatal day 0 (P0) compared to uninjected controls (Figure 2G). By P2, while some individual animals retained detectable C-peptide levels, the group did not show statistically significant elevation compared to uninjected controls. The presence of human C-peptide suggests functional human β-cell activity in the injected mice.

These results demonstrated that injected human pancreatic progenitors can differentiate into insulin-producing cells in *Pdx1*$^{-/-}$ mice.

Human pancreatic cells engraft and express pancreatic genes in the duodenum of *Pdx1*$^{-/-}$ newborns

Although the injected pancreatic cell-deficient mice survived significantly longer, pancreatic structures in their bodies were not observed (Figure 2E). Therefore, we investigated the ectopic engraftment of human pancreatic cells (Figure 3A). Several studies have reported that pancreatic cells can arise ectopically because of deficiencies in transcription factors essential for pancreatic development. Pancreatic endocrine cells have been observed in the spleen of *Ptf1a* knockout mice (Krapp et al., 1998). In addition, pancreatic cells have been found in the stomach, duodenum, and bile duct of *Hes1* knockout mice (Fukuda et al., 2006). We employed droplet digital PCR (ddPCR) to quantify human cell distribution in injected mice. This method enables absolute DNA quantification through partitioning PCR products into nanoliter-sized droplets, demonstrated previously to be effective for chimerism quantification (Suchy et al., 2024, 2022). We established a sensitive human DNA detection system using probes targeting primate-specific (*Caspase7*) and conserved mammalian (*Zeb2*) sequences. The assay was validated using defined mixtures of human and mouse DNA, confirming reliable detection down to 1% human DNA content (Figure S8). Analysis of multiple organs from P0 *Pdx1*$^{-/-}$ newborns revealed that the duodenum contained significantly higher proportions of human DNA (2.8 ± 1.2%, mean ± SD, n = 8, $p < 0.01$) compared to uninjected controls, while other organs including truncated pancreas, kidney, intestine, liver, lungs, and spleen showed negligible human DNA content (Figure 3B).

Flow cytometric analysis further confirmed human cell engraftment in the duodenum. We identified CD45.2 and CD31 double-negative (non-hematopoietic, non-endothelial) cells that were positive for both the transgenic human cell marker iRFP and human leukocyte antigen (HLA) in injected samples (Figure 3C). These human-specific marker-positive cells comprised 5.84 ± 2.00% of viable cells in the injected duodenum, significantly higher than in uninjected controls (1.78 ± 0.54%, $p < 0.01$).
Together, these ddPCR and flow cytometric analyses provided complementary evidence for specific human cell engraftment in the duodenum of injected *Pdx1*$^{-/-}$ mice, with minimal distribution to other organs.

Transcriptome analysis demonstrated human cells underwent differentiation after injection

To determine whether the engrafted human cells underwent functional maturation, we performed fluorescence-activated cell sorting (FACS) to isolate HLA and iRFP double-positive cells from the duodenum of injected *Pdx1*$^{-/-}$ mice and compared their transcriptional profiles to the pancreatic progenitor cells used for injection donor (Figure 3D). RNA sequencing analysis was performed with reads mapped to the human genome. PCA demonstrated clear transcriptional divergence between the sorted cells and the progenitors, indicating substantial gene expression changes following engraftment (Figure 3E). DEG analysis revealed significant upregulation of pancreatic endocrine lineage genes in the engrafted cells compared to the starting population (Figure 3F). Engrafted human cells exhibited marked downregulation of pancreatic progenitor-associated genes, indicating progression beyond the progenitor stage (Figure 3G, K). Additionally, key β-cell transcription factors (*PDX1*, *NEUROD1*, *MAFA*, *MAFB*) and functional genes essential for glucose sensing (*GCK*), insulin biosynthesis (*INS*), insulin processing (*PCSK1*), and secretion machinery (*SLC30A8*, *ABCC8*, *KCNJ11*) were robustly upregulated, consistent with β-cell specification and functional maturation (Figure 3H, K). In addition to β-cell markers, elevated expression of α-cell (*GCG*, *ARX*), δ-cell (*SST*), and ε-cell (*GHRL*) genes was observed, whereas *PPY* transcripts were not detected (Figure 3I, K). Expression of acinar (*CPA2*, *AMY2A*) and ductal (*CFTR*) markers in the sorted cells further suggested the presence of a heterogeneous pancreatic lineage composition within the engrafted population (Figure 3J, K).

These transcriptomic analyses demonstrated that the human pancreatic cells engrafted in the duodenum maintained pancreatic identity and underwent differentiation toward more mature endocrine phenotypes including β-like cells, consistent with their ability to produce insulin and support extended survival of *Pdx1*$^{-/-}$ mice.

Transcriptome analysis reveals potential immune modulation in host duodenum after human cell engraftment

To investigate potential effects of human pancreatic progenitor cell engraftment on host tissue, we performed bulk RNA sequencing of duodenal tissue collected at P0 from *Pdx1*$^{-/-}$ mice with or without intraplacental human pancreatic cell injection. Reads were mapped to the mouse genome to exclude human cell-derived transcripts.

DEG analysis revealed substantial transcriptional alterations in the host duodenum following injection. In total, 1695 genes were significantly upregulated and 788 genes were downregulated in the injected group compared to uninjected controls (adjusted $p < 0.05$, |log2 fold change| > 1) (Figure S7A).

KEGG pathway enrichment analyses revealed that pathways related to innate immune responses such as neutrophil extracellular trap formation and cornified envelope were significantly upregulated. Conversely, gene sets associated with allograft rejection, autoimmune thyroid disease were significantly downregulated (Figure S7B). Representative heatmaps demonstrated coordinated upregulation of *Fpr1*, Complement *C3*, Histone component genes, suggesting an activated innate immune system in the duodenal tissue (Figure S7C). On the other hand, allograft rejection through T cells was suggested to be suppressed by coordinated downregulation of T cell receptor *Cd28*, *Fas*, and a series of MHC class I genes (Figure S7D). Interestingly, fat digestion and absorption were significantly downregulated (Figure S7B). Representative heatmaps demonstrated coordinated downregulation of intestinal absorption–related genes such as *Abcg8*, *Npc1l1*, *Apoa4*, and *Dgat1*, suggesting the incorporation of human cell might have impaired digestive function (Figure S7E).

Taken together, these transcriptomic findings suggest that xenogeneic cell injection might have altered the local epithelial and immune environment of the developing mouse intestine.

IHC detected insulin-positive cell ectopic engraftment in *Pdx1*$^{-/-}$ newborns duodenum

To directly visualize the engrafted human cells and their functional properties, we performed immunohistochemistry on duodenal sections from injected *Pdx1*$^{-/-}$ newborns. Multiple insulin-positive cells were detected within the duodenal villi of injected samples across different individuals (Figure 4B, D). Since *Pdx1*$^{-/-}$ mice lack endogenous pancreatic tissue and cannot produce insulin on their own, the presence of insulin-positive cells in the duodenum provided strong evidence that the injected human pancreatic progenitor cells not

only engrafted but also differentiated into insulin-producing cells. Control duodenal sections from uninjected *Pdx1*$^{-/-}$ mice showed no insulin-positive cells (Figure 4C, D).

To rule out the possibility that human cells remained in the placenta and contributed to circulating human insulin, we analyzed placental tissues from injected embryos. WT mice were subjected to intraplacental injection and placental samples were collected at E18.5 via cesarean section to prevent maternal consumption. ddPCR analysis did not detect human DNA above background levels in placental samples (n = 13), confirming that injected cells did not significantly remain in the placenta (Figure S9B). RT-qPCR analysis of these placental samples showed no detectable expression of human *INS* (Figure S9C). The absence of insulin expression in placenta indicated that the human C-peptide detected in P0 serum samples must originate from human cells that were engrafted outside the placenta, most likely the insulin-positive cells we identified in the duodenum.

These immunohistochemical observations, together with our ddPCR, flow cytometry, and transcriptomic analysis, provided evidence that human pancreatic progenitor cells transplanted via intraplacental injection can engraft in the *Pdx1*$^{-/-}$ mouse duodenum and differentiate into functional insulin-producing cells, which contributed to the extended survival of these pancreas-deficient mice.

Discussion

Our study demonstrated the successful transplantation of human iPSC-derived pancreatic progenitor cells into mouse embryos via intraplacental injection. We established reproducible protocols for generating PDX1+ pancreatic progenitors with consistent differentiation efficiency and demonstrated their capacity to further differentiate into hormone-producing cells *in vitro*. Upon injection, the injected human cells predominantly localized to the duodenum where they expressed pancreatic genes and produced insulin, extending the lifespan of *Pdx1*$^{-/-}$ mice from less than 1 day to up to 10 days after birth. Through multiple complementary analyses, including ddPCR, flow cytometry, immunohistochemistry, and transcriptome profiling, we confirmed the engraftment and functionality of human cells in the mouse neonatal environment. This *in vivo* functional validation provided evidence that specified human pancreatic progenitors can integrate into a developing mouse embryo and contribute to physiological functions, demonstrating the potential for creating interspecies chimeras with functional human-derived tissues.

Our approach differs from previous interspecies complementation studies that used blastocyst injection of pluripotent stem cells. Kobayashi et al. demonstrated that rat

pluripotent stem cells injected into Pdx1-deficient mouse blastocysts generated structurally complete rat-derived pancreas in the host mouse, enabling survival beyond the neonatal period (Kobayashi et al., 2010). Similarly, Wu et al. showed efficient rat-mouse chimerism through blastocyst complementation, with chimeric contribution to multiple tissues (Wu et al., 2017). These studies utilized early-stage embryo injection of pluripotent cells, allowing broader developmental integration throughout embryogenesis. In contrast, our study introduced lineage-committed progenitor cells at a mid-gestation timepoint (E9.5), when the developmental trajectory is already substantially established. The use of lineage-committed progenitors rather than pluripotent stem cells offers several advantages. First, it minimizes the potential for unintended differentiation into other lineages, particularly germ cells and central nervous system, thus reducing ethical concerns associated with human-animal chimeras. Second, it provides a more directed approach for studying the integration and function of specific cell types. However, this strategy has limitations, as evidenced by the incomplete rescue of the *Pdx1*$^{-/-}$ phenotype and lack of structural pancreatic organization. The contrasting outcomes between our approach and blastocyst complementation highlight the importance of developmental timing and cellular potency in determining the extent of functional integration in interspecies chimeras.

We observed the engraftment of human pancreatic progenitors in the duodenum. The duodenum expresses *Pdx1* during development (Offield et al., 1996), potentially providing a compatible developmental environment for PDX1+ human progenitor cells. This selective tropism is reminiscent of observations in *Hes1* knockout mice, where pancreatic cells develop ectopically in the stomach, duodenum, and bile duct (Fukuda et al., 2006), suggesting that epithelial cells in the digestive tract may share a developmental trajectory with pancreatic cells. The vascular connection between the placenta and developing organs likely plays a crucial role in cell distribution after intraplacental injection. At E9.5, the embryonic vascular system is established but still developing. The duodenum receives substantial blood flow through the superior mesenteric artery, which develops through extensive remodeling of the vitelline artery system and achieves functional capacity by this developmental stage (Downs et al., 1998). The omphalomesenteric circulation dominates over umbilical circulation until E9.5, directing substantial perfusion volume toward developing digestive organs (Hatch and Mukouyama, 2015; Walls et al., 2008) . Our previous publication demonstrated that intraplacental injection of AAV9 resulted in widespread transduction across multiple organs, with particularly high efficiency in intestinal tissue, suggesting that the duodenum may indeed have advantageous blood flow characteristics (Gogoleva et al., 2023). This vascular architecture may facilitate the delivery of injected cells

368 to the duodenal region. Further research using lineage tracing and real-time imaging could
369 elucidate the precise mechanisms governing this selective cell engraftment.

370 Despite extending the lifespan of *Pdx1*$^{-/-}$ mice, the transplanted human cells provided only
371 partial functional rescue. Several factors likely contribute to this limited efficacy. First, the
372 relatively low percentage of engrafted human cells is likely insufficient to fully compensate
373 for the absence of an entire pancreas. Second, the engrafted cells did not organize into a
374 structured pancreatic tissue with proper islet architecture, which is crucial for coordinated
375 hormone secretion and glucose homeostasis. Immune-mediated rejection may also limit the
376 long-term function of human cells. Our transcriptomic analysis of mouse duodenum
377 suggested upregulation of genes associated with innate immune responses. These
378 transcriptional changes suggest that xenogeneic cell presence may elicit a localized innate
379 immune reaction, even in the absence of adaptive immune activation. Previous works have
380 highlighted the importance of the CD47-SIRPα axis in xenograft rejection by macrophages
381 (Azimzadeh et al., 2015; Ide et al., 2007), and innate immune mechanisms can act even in
382 prenatal period. The use of SIRPα-humanized mice, which enable cross-species recognition
383 of CD47, has been shown to reduce macrophage-mediated phagocytosis and enhance
384 human cell engraftment *in vivo* (Jinnouchi et al., 2020). The absence of this compatibility in
385 our model may contribute to the challenges in achieving sustained metabolic function, as
386 evidenced by the variable glucose regulation patterns, human C-peptide levels and limited
387 survival extension. Incorporating such immunomodulatory strategies will be critical for future
388 efforts aimed at achieving stable and functional human cell integration.

389 Our study provided a proof-of-concept for human-animal chimera research using
390 lineage-committed progenitor cells and intraplacental injection. This approach represents a
391 technically accessible and ethically sound alternative to blastocyst complementation for
392 studying human cell development and function *in vivo*. The high survival rate of injected
393 embryos (>80% at optimal cell concentrations) overcomes previous limitations of *in utero*
394 injection systems, enabling efficient delivery of human cells to developing embryos.

395 Several strategies could enhance the efficacy of this approach in future studies. Using
396 immunodeficient recipients could reduce rejection and promote longer-term survival of
397 human cells. Alternative recipient models with more selective defects, such as *Ngn3*$^{-/-}$ mice
398 lacking only endocrine pancreatic cells (Gradwohl et al., 2000), might allow more focused
399 study of endocrine function without complete pancreatic agenesis. Additionally, engineering
400 donor cells to express factors that enhance survival, such as anti-apoptotic genes or
401 immunomodulatory molecules, could improve engraftment efficiency.

In conclusion, our study demonstrated the feasibility of generating interspecies chimeras with functional human pancreatic cells through *in utero* transplantation of lineage-committed progenitors. While the rescue of the *Pdx1*$^{-/-}$ phenotype was incomplete, this work establishes a foundation for developing more sophisticated human-animal chimera models for studying human development and testing regenerative therapies. Future refinements in cell delivery, recipient selection, and donor cell engineering will likely enhance the utility of this approach for both basic research and translational applications.

Experimental Procedures

Animals

WT B6D2F1 (BDF1) mice were obtained from The Jackson Laboratory, Yokohama, Japan. Pdx1-LacZ heterozygous (*Pdx1*$^{+/-}$) mice (Offield et al., 1996) were crossed with BDF1 mice for more than 10 generations to generate hybrids, as the better proliferation of hybrid strains was preferable. All mice were maintained under specific pathogen-free conditions at the University of Tsukuba Laboratory Animal Resource Center. All experiments were performed under relevant Japanese and institutional laws and guidelines and were approved by the University of Tsukuba Animal Ethics Committee (authorization number 23–039).

Genotyping

Genotypes were assessed by PCR analysis of tail DNA. For genotyping, the primers for *Pdx1* loci were as follows: Pdx1_FW 5′-ATTGAGATGAGAACCGGCATG-3′, Pdx1-LacZ_FW 5′-TGTGAGCGAGTAACAACC-3′, and Pdx1_RV 5′-TTCATGCGACGGTTTTGGAAC-3′. *Pdx1*$^{-/-}$ embryos, the injection recipients, were obtained by mating *Pdx1*$^{+/-}$ mice. The presence of a vaginal plug was checked the morning following mating, and the mice were considered to be carrying E0.5 embryos.

Generation of PDX1-tdTomato and EEF1A1-iRFP670 iPS lines using genome editing technology

The PDX1-tdTomato and EEF1A1-iRFP670 iPS lines were generated using genome editing technology modified from our method published in a previous study (Nakade et al., 2023). Briefly, the expression vector for Cas9 nuclease and the guide RNA for cleaving the PDX1 gene (RDB20280: pX330-PDX1) were constructed by inserting annealed synthetic oligomers (5′-CACCgcagctcctgcctctcatcg-3′ and 5′-AAACcgatgagaggcaggagctgc-3′) into the Bbs I site of pX330-U6-Chimeric_BB-CBh-hSpCas9 vector (#42230; Addgene, Watertown, MA, USA; a gift from Prof. Feng Zhang). To construct the donor vector, a part of the human PDX1 gene

434 corresponding to 1 kb up- and downstream of the stop codon was amplified by PCR using a
435 primer set (PDX1_LAf: 5′-actgcaggttgcacccattcgcagg-3′ and PDX1_RAr:
436 5′-gccttgcaagatgttctcttcctcag-3′) and genomic DNA from WI38 cells as a template. The PCR
437 product was cloned into the KpnI site of the pCRtk2×2NN vector (RDB18670) to generate
438 pCRtk-PDX1 using an In-Fusion HD Cloning Kit (639648; Takara Bio Inc., Shiga, Japan).
439 Subsequently, pCRtk2X2-PDX1 was amplified into two fragments by PCR using two primer
440 sets (PDX1 LAr and p15AoriF and PDX1 RAf and p15AoriR). To prepare the
441 reporter-selection marker, a part of the pUC-TEZ vector (RDB18672) harboring the
442 P2A-tdTomato and EF1 alpha promoter-driven bleomycin resistance gene was amplified by
443 PCR using the 2Af-1-16 and Bleo-R inf-puro primer set. PCR fragments were subjected to
444 In-Fusion cloning to generate pUCtk-PDX1-TbsdEZ (RDB20281). The DNA sequences of all
445 constructed plasmids were confirmed using a 3500 Genetic Analyzer (Applied Biosystems,
446 Foster City, CA, USA).

447 To generate the EEF1A1-iRFP670 iPSC line, the expression vector for Cas9 nuclease and
448 the guide RNA for cleaving the EEF1A1 gene, previously described as pX459-gEEF1A1
449 (RDB19570 deposited in the RIKEN DNA bank) (Nakade et al., 2023). The methods for
450 constructing the donor vector for iRFP670 insertion were the same as those for
451 PDX1-tdTomato, described previously. The iRFP670 sequence was cloned into
452 pNLS-iRFP670 (#45466; Addgene) (Shcherbakova and Verkhusha, 2013). The resulting
453 vector, pCRtk-EEF1A1-iRFP670-BSD (RDB20282), was used as the donor vector.

454 To generate knock-in cells, 5 μg of the donor vector and 1 μg of the Cas9-gRNA expression
455 vector were introduced into 1 × 10^6 cells of 1383D6 human iPSCs using an electroporator
456 (NEPA21; Neppa Gene Co., Ltd., Chiba, Japan). Four days after electroporation, the
457 electroporated cells underwent zeocin selection at 2 μg/mL. Since HSV-tk expression
458 cassettes, designed outside left and right homology arms, were included in the donor vector,
459 30 μg/mL of ganciclovir was used to exclude clones with random insertions.

460 For the single-cell-derived colony cloning of PDX1-tdTomato clones, antibiotic-resistant cells
461 were expanded to 100 cells/cm^2 to isolate single-cell-derived colonies. Thirty-six isolated
462 clones were examined for the presence of targeted insertion by PCR using PDX1_SeqUpLA:
463 5′-ATTTGCTGGCTCTCAGGTTGGGACT-3′ and PDX1_seqRA:
464 5′-GTTGAAGCCCCTCAGCCAGGAGCAG-3′. All 36 clones tested positive for the targeted
465 insertion. For further experiments, we selected one clone as the PDX1-P2A-tdTomato line,
466 which was deposited in the RIKEN Cell Bank as HPS4904. For the single-cell-derived colony
467 cloning of the EEF1A1-iRFP670 line, antibiotic-resistant and iRFP670-positive cells were
468 expanded to 100 cells/cm2 to isolate single-cell-derived colonies. Twelve Isolated clones

were examined for the presence of targeted insertion by PCR using EEF1A1-up_FW: 5′-ACATGCTGGAGCCAAGTGCTA -3′ and EEF1A1-down_Rv: 5′-ATCACACAAACAGAAAGCATGTCC -3′. Eleven of the 12 clones were positive for targeted insertion. For further experiments, we selected one clone as the EEF1A1-iRFP670-TEZ line, which was deposited in the RIKEN Cell Bank as HPS5065.

While this knock-in reporter enables real-time visualization of PDX1 expression, the EF1α-promoter driven bleomycin resistance cassette incorporated into the construct may potentially influence endogenous PDX1 expression levels, localization, or function.

Human iPSC culture

Undifferentiated human iPSCs were maintained in feeder-free StemFit AK02N medium (AK02N; Ajinomoto, Tokyo, Japan) to which iMatrix-511 (NP892-012; Nippi, Inc., Tokyo, Japan) and Y-27632 (Y0503; Sigma-Aldrich, St. Louis, MO, USA) was added 24 h after passage. All iPSCs were expanded to generate a master bank within the first five passages and served for the differentiation culture.

Immunohistochemistry

For cultured cells, cells were fixed with 4% paraformaldehyde (FUJIFILM Wako Pure Chemical Corporation) for 10 minutes at room temperature. After washing with PBS, cells were permeabilized with 0.1% Triton X-100 (Wako) in PBS for 10 minutes and blocked with 1% bovine serum albumin (BSA; Wako) in PBS for 1 hour at room temperature. Primary antibodies were applied overnight at 4°C. Secondary antibodies conjugated with Alexa Fluor 488, 555, or 647 (Thermo Fisher Scientific) were applied for 1 hour at room temperature. Nuclei were counterstained with DAPI using Fluoro-KEEPER Antifade Reagent Non-Hardening Type (Nacalai Tesque). For tissue sections, samples were fixed in Mildform 10N (133-10311; FUJIFILM Wako Pure Chemical Corporation) and paraffinized. Paraffinized tissue blocks were sliced at a 4-μm thickness using a Sliding Microtome SM2000R (Leica Biosystems, Wetzlar, Germany). Samples were incubated in Antigen retrieval buffer (S1699; Agilent Technologies, Santa Clara, CA, USA) for 10 min at 110°C. After blocking with 5% goat serum/1% bovine serum albumin/PBS and Mouse on Mouse blocking reagent (Vector Laboratories, Newark, CA, USA), the samples were incubated with primary antibodies overnight at 4°C. Samples were washed in PBST for 10 minutes three times. Secondary antibodies conjugated with Alexa Fluor 488, 555, or 647 (Thermo Fisher Scientific) were applied for 1 hour at room temperature. Samples were washed in PBST for 10 minutes three times. Nuclei were counterstained with DAPI using Fluoro-KEEPER Antifade Reagent Non-Hardening Type (Nacalai Tesque).Tissue sections were mounted using VECTASHIELD

503 Vibrance Antifade Mounting Medium (Vector Laboratories). Antibodies used were listed in
504 Table S3. All samples were observed under a BIOREVO BZ-X800 microscope (Keyence,
505 Osaka, Japan). All images were adjusted using Lightroom (Adobe, San Jose, CA, USA) and
506 quantified using ImageJ software (NIH, Bethesda, MD, USA).

507 Characterization of human iPSC lines

508 To validate pluripotency, undifferentiated human iPSCs were assessed for pluripotency
509 marker expression through immunocytochemistry. The differentiation potential of
510 established iPSC lines was evaluated through embryoid body formation. Approximately 1.2 ×
511 10^6 cells were suspended in StemFit AK02N supplemented with 12 μL of 10 mM Y-27632
512 and seeded into V-shaped 96-well plates to promote aggregate formation. After 2 days, cell
513 aggregates were transferred to DMEM high glucose (Nacalai Tesque) supplemented with
514 10% fetal bovine serum (Biosera) and cultured for 8 days in suspension. Subsequently,
515 embryoid bodies were plated onto 0.1% gelatin-coated dishes and maintained for an
516 additional 8 days to allow spontaneous differentiation. On day 16, samples were fixed and
517 processed for immunocytochemistry using lineage-specific markers representing the three
518 germ layers. All antibodies used were listed in Table S3.

519 Human iPSC differentiation culture to pancreatic progenitor

520 The culture medium used for the differentiation of PDX1-expressing cells comprised
521 penicillin/streptomycin (P4333; Sigma-Aldrich) added to a basal medium (StemFit or
522 Improved Minimum Essential Medium [IMEM]). On day 0, human iPSCs were seeded at
523 2,500 cells/cm^2 in StemFit AK02N supplemented with iMatrix-411 (0.25 μg/cm^2, NP892-041;
524 Nippi, Inc.), iMatrix-511 (0.25 μg/cm^2), and Y-27632 (10 μM). On day one, the medium was
525 replaced by StemFit AK02N (A + B) supplemented with CHIR99021 (3 μM, #72052;
526 STEMCELL Technologies, Vancouver, BC, Canada) and ActivinA (10 ng/mL) (725748-11-8;
527 Fujifilm Wako Pure Chemical Corporation, Osaka, Japan). On day three, the medium was
528 replaced by StemFit AK02N (A + B) supplemented with activin A (10 ng/mL). On day 5, the
529 medium was changed to Modified IMEM with L-glutamine (A1048901; Thermo Fisher
530 Scientific, Waltham, MA, USA) supplemented with B-27 (1% v/v, 17504044; Thermo Fisher
531 Scientific), retinoic acid (2 μmol/L, R2625; Sigma-Aldrich), cyclopamine-KAAD (0.25 μmol/L,
532 #20943; Cayman Chemical Company, Ann Arbor, MI, USA), SB431542 (10 μM, #72232;
533 STEMCELL Technologies), and DMH-1 (10 μM, 4126/10; R&D Systems, Minneapolis, MN,
534 USA).

For validation of PDX1 expression during pancreatic differentiation, cells at day 11 of differentiation were fixed and PDX1 protein was stained. Images were captured using a BZ-X800 fluorescence microscope (Keyence) with consistent exposure settings across samples at 20× magnification. Quantitative colocalization analysis between stained PDX1 and tdTomato reporter expression was performed using ImageJ software (version 1.54p, NIH, Bethesda, MD, USA) with the Coloc2 plugin. Twenty-five fields from differentiated cell cultures were analyzed. Colocalization was quantified using Manders threshold-corrected coefficients (tM1 and tM2) with Costes auto-threshold regression method to minimize background interference. Colocalization data was visualized using R software (version 4.4.2).

Extended pancreatic organoid culture

To assess the endocrine differentiation potential of PDX1-positive progenitor cells, we employed a three-dimensional organoid culture system with maturation factors. On days 11-13 of the differentiation protocol, cells were harvested by washing with Dulbecco's PBS followed by dissociation with 1 mL Tryple Express (Thermo Fisher Scientific, 2604-013) for 5 minutes at 37°C. Dissociated cells were collected, centrifuged at 200 × g for 3 minutes, and resuspended in pancreatic progenitor medium supplemented with 10 μM Y-27632. Cell suspensions were seeded into V-bottom 96-well plates (EZ-BindShut II, IWAKI, 4420-800LP) at 100 μL per well using multichannel pipettes, then centrifuged at 200 × g for 3 minutes to promote aggregate formation. On the following day, aggregates were cultured in pancreatic organoid medium consisting of Improved DMEM or Advanced DMEM supplemented with B-27 supplement (1% v/v), recombinant human betacellulin (20 ng/mL, 261-CE-010, R&D Systems), exendin-4 (2 μM, 055-09391, Wako), and 3,3',5-triiodo-L-thyronine sodium salt (20 μM, 038-25541, Wako). Medium was changed every other day by aspirating half the volume and adding fresh organoid medium. After two weeks of organoid culture, samples were collected for histological analysis by embedding in IP Gell (Genostaff) followed by fixation with 4% paraformaldehyde.

Flow cytometric analysis

For evaluation of pancreatic differentiation efficiency, cells were harvested at specific timepoints and processed for flow cytometric analysis. At day 3 of differentiation, definitive endoderm formation was assessed using antibodies against CD117 (c-Kit) and CXCR4 (CD184). Cells were dissociated using TrypLE Express (Thermo Fisher Scientific) for 15 minutes at 37°C, collected in PBS containing 10% FBS, and centrifuged at 200 × g for 3 minutes. Cell pellets were resuspended in FACS buffer (1% FBS in PBS) and incubated with

PE anti-human CD117 (BioLegend) and APC anti-human CXCR4 (BioLegend) antibodies at 5 μL per million cells for 30 minutes at room temperature. Following two washes with FACS buffer, cells were resuspended in 200 μL FACS buffer containing DAPI (DOJINDO) for viability assessment.

For pancreatic progenitor evaluation at days 11-14, NKX6-1 expression was analyzed using intracellular staining. Cells were dissociated with Accutase (Nacalai Tesque) for 15 minutes at 37°C, fixed with BD Cytofix fixation buffer (Cat. No. 554655) for 15-30 minutes at 4°C, and permeabilized using BD Phosflow Perm Buffer III (Cat. No. 558050) for 30 minutes on ice. Cells were then incubated with Alexa Fluor 488 Mouse Anti-NKX6-1 antibody (Cat. No. 567608, BD Biosciences) for 15 minutes on ice, followed by two washes with FACS buffer before analysis.

For analysis of human cell engraftment in injected mice, the duodenum of newborn mice was dissociated using collagenase type V (032-17854; FUJIFILM Wako Pure Chemical Corporation) following a published protocol (Uniken Venema et al., 2022). Single-cell suspensions were filtered through 40-μm cell strainers and resuspended in PBS containing 2% fetal bovine serum. Human cells were identified by dual-positive expression of HLA and the constitutive iRFP670 reporter, with additional exclusion of hematopoietic (CD45.2+) and endothelial (CD31+) lineages to focus on non-vascular engrafted cells.

Data acquisition was performed using CytoFLEX (Beckman Coulter). Data analysis was conducted using CytoExpert (Beckman Coulter) and FlowJo software (TreeStar Inc., Ashland, OR, USA). All antibodies used are summarized in Table S3.

Reverse transcription-quantitative PCR

Total RNA was collected using an ISOGEN (Cat. No. 311-02501; Nippon Gene, Tokyo, Japan). cDNA was synthesized using a QuantiTect Reverse Transcription Kit (Cat. No. 205313; Qiagen, Hilden, Germany). Gene expression levels were determined using RT-qPCR performed on a Thermal Cycler Dice Real Time System Single TP850 (Takara Bio Inc.) using THUNDERBIRD® SYBR® qPCR Mix (QPS-201; TOYOBO Co., Ltd., Tokyo, Japan). mRNA levels were normalized to those of RPLP0. The primer sequences used were summarized in Table S4.

RNA sequence analysis of human iPSC differentiation

Total RNA was extracted using TRIzol (Thermo Fisher Scientific) following standard protocols. An RNA-seq library was prepared using an NEBNext Ultra II Directional RNA Library Prep Kit (New England Biolabs, Ipswich, MA, USA) after ribosomal RNA (rRNA)

depletion using an NEBNext rRNA Depletion Kit (New England Biolabs). Paired-end (2 × 36 bases) sequencing was performed using a NextSeq500 platform (Illumina, San Diego, CA, USA). The FASTQ files were imported into the CLC Genomics Workbench (version 10.1.1; Qiagen), and the sequence reads were mapped to the human reference genome (hg38). Gene expression was calculated as the total read count normalized to transcripts per million. DEGs were extracted using the criterion of FDR-corrected $p < 0.05$.

RNA sequence analysis of chimeric duodenum

Paired-end (2 × 36 bases) sequencing was performed using the same protocol for the iPSC differentiation experiment. FASTQ files were imported into STAR 2.7.11b. Sequence reads were mapped onto the mouse reference genome (mm10) without allowing a single mismatch (--outFilterMismatchNmax 0) or multimapping (--outFilterMultimapNmax 1). DEGs were extracted using DESeq2 in R (Love et al., 2014) using the criteria of $p < 0.05$ and log2 fold change > 2. GO analysis was performed using clusterprofiler (Wu et al., 2021). Clustering heatmaps were constructed using R software.

FACS sorting and RNA sequencing of human cells

For transcriptome analysis of engrafted human cells, duodenal tissues from injected *Pdx1*$^{-/-}$ newborns were harvested at P0 and processed for FACS. Tissues were dissociated using collagenase type V (032-17854; FUJIFILM Wako Pure Chemical Corporation) as described above, followed by filtration through 40-μm cell strainers to obtain single-cell suspensions. Dead cells were excluded using DAPI staining, and human cells were identified by dual-positive expression of HLA and the iRFP670 reporter. Sorting was performed using a MoFlo XDP sorter (Beckman Coulter). Control samples from uninjected *Pdx1*$^{-/-}$ mice were processed in parallel to account for potential background signals.

RNA sequencing libraries were prepared using the same protocol as above. Paired-end sequencing (2 × 150 bases) was performed on a NextSeq500 platform (Illumina, San Diego, CA, USA). Total RNA was extracted using ISOGEN-LS (NIPPON GENE). Sequence reads were processed using STAR aligner (version 2.7.11b) with Two-pass mapping mode. Reads were mapped exclusively to the human reference genome (hg38) using parameters (outFilterMismatchNoverReadLmax 0.06, outFilterMultimapNmax 10, outFilterMatchNminOverLread 0.3, outFilterScoreMinOverLread 0.3, alignSJoverhangMin 8, alignSJDBoverhangMin 3). DEG analysis was performed using DESeq2 (version 1.34.0) in R, with genes showing log2 fold change > 2 and adjusted p-value < 0.05 considered significantly differentially expressed. DEGs were listed in Table S5.

Intraplacental injection

Intraplacental injection was performed with prior protocols (Jeon et al., 2021). Shortly before injection, the differentiated cells were dissociated using Accutase (12679-54; Nacalai Tesque, Kyoto, Japan) for 15 min at 37°C and washed in PBS twice. The cells were then suspended in cold PBS. Pregnant mice bearing E9.5 embryos were anesthetized with isoflurane while resting on a 37°C heating plate. The uterus was carefully exposed through an abdominal incision. The donor cell suspension was loaded into the injection needle through mouth pipetting using rubber tube (Drummond, 68-0449-50) and subsequently installed to a microinjector (FemtoJet; Eppendorf, Hamburg, Germany). Each placenta was punctured by an injection needle to a depth of 2 mm, and the donor cell suspension was injected at an injection pressure of 60 hPa. After injection, the uterus was carefully repositioned, and the incision was securely closed. After surgery, the mice were placed on a plastic bag containing warm water to prevent hypothermia.

Survival analysis

Individual identification of newborn mice was established by tattooing their limbs on the day of birth. Genotyping was performed using tail-tip samples. Maternal care was enhanced by supplementing the maternal diet with CMF sprouts (Oriental Yeast; Tokyo, Japan). Newborn survival was checked daily until all *Pdx1*$^{-/-}$ mice died. The Kaplan–Meier curve was constructed using GraphPad PRISM 6 (GraphPad Software, La Jolla, CA, USA).

Glucose measurement

A small amount of blood was collected daily via facial vein puncture. Blood glucose levels were measured using a glucometer (Terumo, Tokyo, Japan). The minimum detection limit is 20 mg/dL and all glucose levels lower than the limit are recorded as 20 in our figure 2F.

ELISA assay

ELISA was conducted using a Mercodia Ultrasensitive C-peptide ELISA kit (#10-1141-01; Mercodia, Uppsala, Sweden). Blood samples were collected from P0 and P2 *Pdx1*$^{-/-}$ mice by decapitation. Approximately 25 μL of serum was obtained from each animal and diluted 4-fold with the kit's calibrator diluent to achieve the required 100 μL sample volume for the assay. For the ELISA procedure, calibrator, control, and diluted sample volumes of 100 μL each were added to their respective wells according to the manufacturer's protocol. The plate was incubated on a shaker for 1 h at 25°C and then washed six times with 350 μL of wash buffer. Subsequently, 200 μL of the enzyme conjugate solution was added to each well, followed by another 1 hour incubation on the plate shaker at room temperature. The

plate was then rewashed six times, and 200 μL of TMB substrate was added to each well, followed by a 30 minutes incubation on the bench at room temperature protected from light. Next, 50 μL of stop solution was mixed into each well to terminate the reaction. Optical density readings were obtained at 450 nm using a microplate reader (SpectraMax M5, Molecular Devices) within 30 min. Baseline signals from uninjected control samples were used as assay controls, and only values significantly above this baseline ($p < 0.05$, Student's t-test) were interpreted as positive detection of human C-peptide. All samples were measured in duplicate, and the mean values were used for analysis.

ddPCR analysis

For ddPCR analysis, a QX200 Droplet Digital PCR system (Bio-Rad Laboratories, Hercules, CA, USA) was used. Briefly, to prepare DNA, tissue lysis was conducted in 10% proteinase K solution in a 1% SDS buffer. The samples were incubated at 55°C overnight. The following morning, another round of lysis buffer was added, and incubation was continued for a few additional hours. Proteinase K inactivation was accomplished at 75°C for 10 min, followed by extraction of 50 μL from each sample. To precipitate SDS, 5 μL of 1 M KCl was added, and the samples were briefly centrifuged at 3,000 × g for 1 min at 4°C. The reaction mixture was prepared using a custom ddPCR assay (#10031276 for FAM and #10031279 for HEX; Bio-Rad Laboratories) and ddPCR Supermix for Probes (no dUTP) (#186-3023; Bio-Rad Laboratories) according to the manufacturer's instructions. Droplet formation was performed using droplet generator oil (#186-3005; Bio-Rad Laboratories). The subsequent PCR reaction involved enzyme activation at 95°C for 10 min, denaturation at 94°C for 30 s, and annealing/extension at 60°C for 1 min. This PCR cycle was repeated 50 times, and enzyme deactivation was achieved at 98°C for 10 min, with a final holding step at 12°C. QuantaSoft software (Bio-Rad Laboratories, version 1.7) was used to quantify the absolute number of DNA copies in all wells for data acquisition and analysis. Mouse DNA and human DNA were used to supervise thresholds.

The sequences of primers and probes used are as follows:

chCasp7:

Fw-GAAGAAGAAAAATGTCACCATGCG, Rv-TTTCAAAATTCATGTTGTACTGATATGTAG, Probe-AGACCACCCGGGACCGAGTGCCT

Zeb2:

Fw-GGATGGGGAATGCAGCTCTT, Rv-AGTGCGGCAGAATACAGCA, Probe-TGATGGGTTGTGAAGGCAGCTGCACCT

For validation of these primers and probes, human DNA from EEF1A-iRFP670 and mouse DNA from tail tips were used. DNA was mixed with known ratio (0, 1, 10, 50, 100% human DNA) and served to benchmark its accuracy (Figure S8).

Placental tissue analysis

Pregnant WT mice that had received intraplacental injection of human pancreatic progenitor cells at E9.5 were subjected to cesarean section at embryonic day 18.5 to collect placental tissues before potential maternal consumption. Placentas were carefully dissected from the uterine wall, rinsed with cold PBS to remove maternal blood, and immediately processed for downstream analysis. For DNA extraction, placental tissues were minced and subjected to tissue lysis before proceeding to ddPCR analysis as described above.
For RNA analysis, total RNA was extracted using ISOGEN (NIPPON GENE) following the manufacturer's protocol. Quantitative RT-PCR was performed to detect human insulin (INS) mRNA expression. Human INS ORF plasmid was served as positive control. Duodenum from no-injection newborn was served as negative control.

Statistical analysis

Statistical analyses were performed using R (version 4.4.2) and GraphPad PRISM 6 software. The statistical significance of survival time was determined using the log-rank test. The statistical significance of the differences between three or more groups was determined using one-way ANOVA followed by Tukey–Kramer's multiple comparisons. The statistical significance of the quantification of the immunohistochemistry was determined using Mann-Whitney U test. Statistical methods specific to RNA-sequencing data are described in their respective sections. The statistical significance of the FACS analysis was determined using Welch's t-test. Statistical significance was considered at $p < 0.05$.

Resource availability

Lead contact

Michito Hamada, Ph.D., Department of Anatomy and Embryology, Faculty of Medicine, University of Tsukuba, 1-1-1 Tennodai, Tsukuba 305-8575, Japan; Phone: +81-298-53-7516, Fax: +81-298-53-6965, E-mail: hamamichi@md.tsukuba.ac.jp

Materials availability

This study did not generate new unique reagents.

Data and code availability

RNAseq data was deposited as accession number DRR545160-DRR545181.

Additional metadata, culture details and basic characterization of the cell lines were deposited to RIKEN Cell Bank, as HPS4904 (PDX1-P2A-tdTomato) and HPS5065 (EEF1A1-iRFP670).

Acknowledgments

We thank Dr. Yoshihiro Miwa, Dr. Koji Nakade, Dr. Kenichi Nakashima, and Mrs. Yasuko Hemmi for their technical support in generating PDX-P2A-tdTomato and EEF1A1-iRFP670 hiPSC lines. We thank Dr. Satoshi Yamazaki for providing *Pdx1*$^{LacZ/+}$ mice and technical support for the flow cytometric analysis. We are grateful to all former and current members of the Department of Anatomy and Embryology for their support in all aspects. This work was supported by JSPS KAKENHI (Grant Number JP22H04922, 23K05586, 23K18208), JST (Grant Number JPMJPF2017), AMED (Grant number 23bm1423010h0001), and Research Fellowships of Japan Society for the Promotion of Science for Young Scientists (23KJ0238).

Author contributions

Conceptualization, S.T., Y.H., M.H.; data curation, A.W.; formal analysis, A.W., Z.J.S.; funding acquisition, S.T., A.W., Y.H., H.N.; investigation, A.W., H.J., Z.J.S., T.H., C.W.L., N.G., A.N., Y.H., F.S. Y.A.; methodology, A.W., H.J., M.H., Y.H., F.S.; project administration, A.W., M.H., S.T.; resources, S.T., Y.H., H.N.; software, A.W., T.H.; supervision, S.T., M.H.; validation, A.W., H.J., Z.J.S., T.H., C.W.L., N.G., A.N., Y.H., F.S.; visualization, A.W., Z.J.S., M.H.; writing-original draft, A.W.; writing-review & editing, A.W., H.J., Z.J.S., T.H., C.W.L., N.G., A.N., F.S., H.N., Y.H., M.H., S.T.

Declaration of interests

The authors declare no competing interests.

Declaration of generative AI and AI-assisted technologies in the writing process

During the preparation of this work, the authors used Claude 4 Sonnet in order to improve language and readability. After using this tool/service, the authors reviewed and edited the content as needed and take full responsibility for the content of the publication.

References

Augsornworawat, P., Maxwell, K.G., Velazco-Cruz, L., Millman, J.R., 2020. Single-Cell Transcriptome Profiling Reveals β Cell Maturation in Stem Cell-Derived Islets after Transplantation. Cell Rep. 32, 108067. https://doi.org/10.1016/j.celrep.2020.108067

Azimzadeh, A.M., Kelishadi, S.S., Ezzelarab, M.B., Singh, A.K., Stoddard, T., Iwase, H.,

Zhang, T., Burdorf, L., Sievert, E., Avon, C., Cheng, X., Ayares, D., Horvath, K.A., Corcoran, P.C., Mohiuddin, M.M., Barth, R.N., Cooper, D.K.C., Pierson, R.N., 3rd, 2015. Early graft failure of GalTKO pig organs in baboons is reduced by expression of a human complement pathway-regulatory protein. Xenotransplantation 22, 310–316.

Byrnes, L.E., Wong, D.M., Subramaniam, M., Meyer, N.P., Gilchrist, C.L., Knox, S.M., Tward, A.D., Ye, C.J., Sneddon, J.B., 2018. Lineage dynamics of murine pancreatic development at single-cell resolution. Nat. Commun. 9, 3922. https://doi.org/10.1038/s41467-018-06176-3

Cohen, M.A., Wert, K.J., Goldmann, J., Markoulaki, S., Buganim, Y., Fu, D., Jaenisch, R., 2016. Human neural crest cells contribute to coat pigmentation in interspecies chimeras after in utero injection into mouse embryos. Proc. Natl. Acad. Sci. U. S. A. 113, 1570–1575.

Cohen, M.A., Zhang, S., Sengupta, S., Ma, H., Bell, G.W., Horton, B., Sharma, B., George, R.E., Spranger, S., Jaenisch, R., 2020. Formation of Human Neuroblastoma in Mouse-Human Neural Crest Chimeras. Cell Stem Cell 26, 579–592.e6. https://doi.org/10.1016/j.stem.2020.02.001

Crane, A.T., Voth, J.P., Shen, F.X., Low, W.C., 2019. Concise Review: Human-Animal Neurological Chimeras: Humanized Animals or Human Cells in an Animal? Stem Cells.

Downs, K., Gifford, S., Blahnik, M., Gardner, R.L., 1998. Vascularization in the murine allantois occurs by vasculogenesis without accompanying erythropoiesis. Development 125, 4507–4520.

Fleischman, R.A., Mintz, B., 1979. Prevention of genetic anemias in mice by microinjection of normal hematopoietic stem cells into the fetal placenta. Proc. Natl. Acad. Sci. U. S. A. 76, 5736–5740. https://doi.org/10.1073/pnas.76.11.5736

Fujiki, Y., Fukawa, K., Kameyama, K., Kudo, O., Onodera, M., Nakamura, Y., Yagami, K.-I., Shiina, Y., Hamada, H., Shibuya, A., Nakauchi, H., 2003. Successful multilineage engraftment of human cord blood cells in pigs after in utero transplantation. Transplantation 75, 916–922. https://doi.org/10.1097/01.TP.0000057243.12110.7C

Fukuda, A., Kawaguchi, Y., Furuyama, K., Kodama, S., Horiguchi, M., Kuhara, T., Koizumi, M., Boyer, D.F., Fujimoto, K., Doi, R., Kageyama, R., Wright, C.V.E., Chiba, T., 2006. Ectopic pancreas formation in Hes1 -knockout mice reveals plasticity of endodermal progenitors of the gut, bile duct, and pancreas. J. Clin. Invest. 116, 1484–1493. https://doi.org/10.1172/JCI27704

Gogoleva, N., Shahri, Z.J., Noda, A., Liao, C.-W., Wakimoto, A., Inoue, Y., Jeon, H., Takahashi, S., Hamada, M., 2023. Intraplacental injection of AAV9-CMV-iCre results in the widespread transduction of multiple organs in double-reporter mouse embryos. Exp. Anim. 72, 460–467. https://doi.org/10.1538/expanim.23-0044

Goto, T., Hara, H., Sanbo, M., Masaki, H., Sato, H., Yamaguchi, T., Hochi, S., Kobayashi, T., Nakauchi, H., Hirabayashi, M., 2019. Generation of pluripotent stem cell-derived mouse kidneys in Sall1-targeted anephric rats. Nat. Commun. 10, 451.

Gradwohl, G., Dierich, A., LeMeur, M., Guillemot, F., 2000. neurogenin3 is required for the development of the four endocrine cell lineages of the pancreas. Proceedings of the National Academy of Sciences 97, 1607–1611.

Hamanaka, S., Umino, A., Sato, H., Hayama, T., Yanagida, A., Mizuno, N., Kobayashi, T., Kasai, M., Suchy, F.P., Yamazaki, S., Masaki, H., Yamaguchi, T., Nakauchi, H., 2018. Generation of Vascular Endothelial Cells and Hematopoietic Cells by Blastocyst Complementation. Stem Cell Reports 11, 988–997. https://doi.org/10.1016/j.stemcr.2018.08.015

Hatch, J., Mukouyama, Y.-S., 2015. Spatiotemporal mapping of vascularization and innervation in the fetal murine intestine: Intestinal Neurovascular Patterning. Dev. Dyn. 244, 56–68. https://doi.org/10.1002/dvdy.24178

Hu, Z., Li, H., Jiang, H., Ren, Y., Yu, X., Qiu, J., Stablewski, A.B., Zhang, B., Buck, M.J., Feng, J., 2020. Transient inhibition of mTOR in human pluripotent stem cells enables robust formation of mouse-human chimeric embryos. Sci Adv 6, eaaz0298. https://doi.org/10.1126/sciadv.aaz0298

Ide, K., Wang, H., Tahara, H., Liu, J., Wang, X., Asahara, T., Sykes, M., Yang, Y.-G., Ohdan, H., 2007. Role for CD47-SIRPalpha signaling in xenograft rejection by macrophages. Proc. Natl. Acad. Sci. U. S. A. 104, 5062–5066. https://doi.org/10.1073/pnas.0609661104

Jeon, H., Asano, K., Wakimoto, A., Kulathunga, K., Tran, M.T.N., Nakamura, M., Yokomizo, T., Hamada, M., Takahashi, S., 2021. Generation of reconstituted hemato-lymphoid murine embryos by placental transplantation into embryos lacking HSCs. Sci. Rep. 11, 4374. https://doi.org/10.1038/s41598-021-83652-9

Jinnouchi, F., Yamauchi, T., Yurino, A., Nunomura, T., Nakano, M., Iwamoto, C., Obara, T., Miyawaki, K., Kikushige, Y., Kato, K., Maeda, T., Miyamoto, T., Baba, E., Akashi, K., Takenaka, K., 2020. A human SIRPA knock-in xenograft mouse model to study human hematopoietic and cancer stem cells. Blood 135, 1661–1672.

Kobayashi, T., Goto, T., Oikawa, M., Sanbo, M., Yoshida, F., Terada, R., Niizeki, N., Kajitani, N., Kazuki, K., Kazuki, Y., Hochi, S., Nakauchi, H., Surani, M.A., Hirabayashi, M., 2021. Blastocyst complementation using Prdm14-deficient rats enables efficient germline transmission and generation of functional mouse spermatids in rats. Nat. Commun. 12, 1328. https://doi.org/10.1038/s41467-021-21557-x

Kobayashi, T., Yamaguchi, T., Hamanaka, S., Kato-Itoh, M., Yamazaki, Y., Ibata, M., Sato, H., Lee, Y.-S., Usui, J.-I., Knisely, A.S., Hirabayashi, M., Nakauchi, H., 2010. Generation of rat pancreas in mouse by interspecific blastocyst injection of pluripotent stem cells. Cell 142, 787–799. https://doi.org/10.1016/j.cell.2010.07.039

Krapp, A., Knöfler, M., Ledermann, B., Bürki, K., Berney, C., Zoerkler, N., Hagenbüchle, O., Wellauer, P.K., 1998. The bHLH protein PTF1-p48 is essential for the formation of the exocrine and the correct spatial organization of the endocrine pancreas. Genes Dev. 12, 3752–3763.

Liu, H., Yang, H., Zhu, D., Sui, X., Li, J., Liang, Z., Xu, L., Chen, Z., Yao, A., Zhang, L., Zhang, X., Yi, X., Liu, M., Xu, S., Zhang, W., Lin, H., Xie, L., Lou, J., Zhang, Y., Xi, J., Deng, H., 2014. Systematically labeling developmental stage-specific genes for the study of pancreatic β-cell differentiation from human embryonic stem cells. Cell Res. 24, 1181–1200. https://doi.org/10.1038/cr.2014.118

Loh, K.M., Ang, L.T., Zhang, J., Kumar, V., Ang, J., Auyeong, J.Q., Lee, K.L., Choo, S.H., Lim, C.Y.Y., Nichane, M., Tan, J., Noghabi, M.S., Azzola, L., Ng, E.S., Durruthy-Durruthy, J., Sebastiano, V., Poellinger, L., Elefanty, A.G., Stanley, E.G., Chen, Q., Prabhakar, S., Weissman, I.L., Lim, B., 2014. Efficient endoderm induction from human pluripotent stem cells by logically directing signals controlling lineage bifurcations. Cell Stem Cell 14, 237–252. https://doi.org/10.1016/j.stem.2013.12.007

Maeng, G., Das, S., Greising, S.M., Gong, W., Singh, B.N., Kren, S., Mickelson, D., Skie, E., Gafni, O., Sorensen, J.R., Weaver, C.V., Garry, D.J., Garry, M.G., 2021. Humanized skeletal muscle in MYF5/MYOD/MYF6-null pig embryos. Nature Biomedical Engineering 5, 805–814. https://doi.org/10.1038/s41551-021-00693-1

Ma, H., Wert, K.J., Shvartsman, D., Melton, D.A., Jaenisch, R., 2018. Establishment of human pluripotent stem cell-derived pancreatic β-like cells in the mouse pancreas. Proc. Natl. Acad. Sci. U. S. A. 115, 3924–3929. https://doi.org/10.1073/pnas.1702059115

Masaki, H., Kato-Itoh, M., Umino, A., Sato, H., Hamanaka, S., Kobayashi, T., Yamaguchi, T., Nishimura, K., Ohtaka, M., Nakanishi, M., Nakauchi, H., 2015. Interspecific in vitro assay for the chimera-forming ability of human pluripotent stem cells. Development 1–9.

Nakade, K., Tsukamoto, S., Nakashima, K., An, Y., Sato, I., Li, J., Shimoda, Y., Hemmi, Y., Miwa, Y., Hayashi, Y., 2023. Efficient selection of knocked-in pluripotent stem cells using a dual cassette cellular elimination system. Cell Rep Methods 3, 100662. https://doi.org/10.1016/j.crmeth.2023.100662

Offield, M.F., Jetton, T.L., Labosky, P.A., Ray, M., Stein, R.W., Magnuson, M.A., Hogan, B.L., Wright, C.V., 1996. PDX-1 is required for pancreatic outgrowth and differentiation of the rostral duodenum. Development 122, 983–995.

Pagliuca, F.W., Millman, J.R., Gürtler, M., Segel, M., Van Dervort, A., Ryu, J.H., Peterson, Q.P., Greiner, D., Melton, D.A., 2014. Generation of functional human pancreatic β cells

in vitro. Cell 159, 428–439. https://doi.org/10.1016/j.cell.2014.09.040
Puri, S., Hebrok, M., 2007. Dynamics of embryonic pancreas development using real-time imaging. Dev. Biol. 306, 82–93. https://doi.org/10.1016/j.ydbio.2007.03.003
Rezania, A., Bruin, J.E., Arora, P., Rubin, A., Batushansky, I., Asadi, A., O'Dwyer, S., Quiskamp, N., Mojibian, M., Albrecht, T., Yang, Y.H.C., Johnson, J.D., Kieffer, T.J., 2014. Reversal of diabetes with insulin-producing cells derived in vitro from human pluripotent stem cells. Nat. Biotechnol. 32, 1121–1133. https://doi.org/10.1038/nbt.3033
Shahjalal, H.M., Shiraki, N., Sakano, D., Kikawa, K., Ogaki, S., Baba, H., Kume, K., Kume, S., 2014. Generation of insulin-producing β-like cells from human iPS cells in a defined and completely xeno-free culture system. J. Mol. Cell Biol. 6, 394–408. https://doi.org/10.1093/jmcb/mju029
Shcherbakova, D.M., Verkhusha, V.V., 2013. Near-infrared fluorescent proteins for multicolor in vivo imaging. Nat. Methods 10, 751–754. https://doi.org/10.1038/nmeth.2521
Suchy, F.P., Karigane, D., Nakauchi, Y., Higuchi, M., Zhang, J., Pekrun, K., Hsu, I., Fan, A.C., Nishimura, T., Charlesworth, C.T., Bhadury, J., Nishimura, T., Wilkinson, A.C., Kay, M.A., Majeti, R., Nakauchi, H., 2024. Genome engineering with Cas9 and AAV repair templates generates frequent concatemeric insertions of viral vectors. Nat. Biotechnol. https://doi.org/10.1038/s41587-024-02171-w
Suchy, F.P., Nishimura, T., Seki, S., Wilkinson, A.C., Higuchi, M., Hsu, I., Zhang, J., Bhadury, J., Nakauchi, H., 2022. Streamlined and quantitative detection of chimerism using digital PCR. Sci. Rep. 12, 10223.
Uniken Venema, W.T.C., Ramírez-Sánchez, A.D., Bigaeva, E., Withoff, S., Jonkers, I., McIntyre, R.E., Ghouraba, M., Raine, T., Weersma, R.K., Franke, L., Festen, E.A.M., van der Wijst, M.G.P., 2022. Gut mucosa dissociation protocols influence cell type proportions and single-cell gene expression levels. Sci. Rep. 12, 9897. https://doi.org/10.1038/s41598-022-13812-y
Walls, J.R., Coultas, L., Rossant, J., Henkelman, R.M., 2008. Three-dimensional analysis of vascular development in the mouse embryo. PLoS One 3, e2853. https://doi.org/10.1371/journal.pone.0002853
Wang, H., Yin, X., Xu, J., Chen, L., Karuppagounder, S.S., Xu, E., Mao, X., Dawson, V.L., Dawson, T.M., 2024. Interspecies chimerism with human embryonic stem cells generates functional human dopamine neurons at low efficiency. Stem Cell Reports 19, 54–67. https://doi.org/10.1016/j.stemcr.2023.11.009
Wu, J., Greely, H.T., Jaenisch, R., Nakauchi, H., Rossant, J., Belmonte, J.C.I., 2016. Stem cells and interspecies chimaeras. Nature 540, 51–59. https://doi.org/10.1038/nature20573
Wu, J., Platero-Luengo, A., Sakurai, M., Sugawara, A., Gil, M.A., Yamauchi, T., Suzuki, K., Bogliotti, Y.S., Cuello, C., Morales Valencia, M., Okumura, D., Luo, J., Vilariño, M., Parrilla, I., Soto, D.A., Martinez, C.A., Hishida, T., Sánchez-Bautista, S., Martinez-Martinez, M.L., Wang, H., Nohalez, A., Aizawa, E., Martinez-Redondo, P., Ocampo, A., Reddy, P., Roca, J., Maga, E.A., Esteban, C.R., Berggren, W.T., Nuñez Delicado, E., Lajara, J., Guillen, I., Guillen, P., Campistol, J.M., Martinez, E.A., Ross, P.J., Izpisua Belmonte, J.C., 2017. Interspecies Chimerism with Mammalian Pluripotent Stem Cells. Cell 168, 473–486.e15. https://doi.org/10.1016/j.cell.2016.12.036

Downs, K. M., & Rodriguez, A. M. 2020. The mouse fetal-placental arterial connection: A paradigm involving the primitive streak and visceral endoderm with implications for human development. Wiley Interdisciplinary Reviews. Developmental Biology, 9(2), e362.

Wu, J., & Izpisua Belmonte, J. C. (2016). Stem Cells: A Renaissance in Human Biology Research. Cell, 165(7), 1572–1585.

Figure Legends

Figure 1 Differentiation of pancreatic progenitor and establishment of intraplacental injection. (A) Schematic representation of the stepwise differentiation protocol for generating PDX1+ pancreatic progenitors from human iPSCs. SF: StemFit medium, IMEM: Improved Minimum Essential Medium, CHIR: CHIR99021, Cyc-KAAD: Cyclopamine-KAAD, RA: retinoic acid. (B) Validation of PDX1-tdTomato reporter line. Representative immunofluorescence images showing co-localization of endogenous PDX1 protein (green) and tdTomato reporter (red) expression at day 13 of differentiation. Scale bar: 100 μm. Quantification shows 66.3% ± 7.4% co-localization efficiency after threshold. (C) Left: representative fluorescent microscopic image of differentiated PDX1-tdTomato line at day 13. Right: representative flow cytometric analysis of differentiated PDX1-tdTomato line at day 13. (D) Time-course expression analysis of pancreatic differentiation markers by RT-qPCR. Gene expression levels normalized to *RPLP0* and day 0 control. EEF1A1-iRFP670 line was used. Data shown as mean and each biological replicate, n = 3 independent experiments. (E) Transcriptomic comparison of iPSCs versus differentiated pancreatic progenitors at day 13. Heatmap showing differential expression of key developmental genes between hiPSCs (day 0) and day 13 pancreatic progenitors. Cell line: EEF1A1-iRFP670 line. Statistics: n = 4 biological replicates each condition. (F) Comparison of pancreatic differentiation markers' normalized counts between undifferentiated hiPSCs and day 13 pancreatic progenitors. Cell line: EEF1A1-iRFP670 line. Statistics: n = 4, statistical analysis by DESeq2 Wald test, $*p < 0.05$, ns = not significant, data shown as individual points with mean. (G) Experimental workflow for intraplacental injection studies. Schematic showing cell differentiation timeline coordinated with mouse mating and embryonic injection at E9.5. Cell line: EEF1A1-iRFP670 line. (H) Optimization of cell injection dose for embryonic survival. Birth rates of WT embryos following intraplacental injection of human pancreatic progenitors at various cell concentrations. Cell line: EEF1A1-iRFP670 line. Sample sizes are detailed in Table S1.

Figure 2 Injection of human pancreatic cells supports *Pdx1*$^{-/-}$ newborn mice through insulin secretion. (A) Schematic showing intraplacental injection of human pancreatic progenitors into *Pdx1*$^{+/-}$ mating embryos at E9.5 and E10.5. (B) Kaplan-Meier survival curves comparing *Pdx1*$^{+/-}$ (left panel) and *Pdx1*$^{-/-}$ mice (right panel) with and without human cell injection at E9.5 or E10.5. *Pdx1*$^{+/-}$: no injection n = 10, injected n = 11; *Pdx1*$^{-/-}$: no injection n =4, injected n = 11. Log-rank test, $*p < 0.05$, $**p < 0.01$, ns = not significant. (C) Representative photographs of *Pdx1*$^{+/-}$ and *Pdx1*$^{-/-}$ injected (E9.5 injection) mice at P1 and P4, showing growth differences. Scale bar = 1 cm. (D) Body weight comparison at P0. Data were shown as individual data points with mean ± SEM. Left and middle panel compare different genotypes.

961 Right panel compares *Pdx1*$^{-/-}$ mice with at E9.5 and without injection. No injection; WT, n = 5;
962 *Pdx1*$^{+/-}$, n = 8; *Pdx1*$^{-/-}$, n = 5. Injected; WT, n = 15; *Pdx1*$^{+/-}$, n = 25; *Pdx1*$^{-/-}$, n = 11. Statistical
963 analysis by one-way ANOVA with Tukey's post-hoc test, *$p < 0.05$, **$p < 0.01$, ns = not
964 significant. (E) Representative gross anatomy of internal organs at P0. Comparison between
965 *Pdx1*$^{+/-}$ (left) and *Pdx1*$^{-/-}$ + injection at E9.5 (right) mice showing absence of pancreatic tissue
966 in injected *Pdx1*$^{-/-}$ mice. Scale bar = 1 cm. (F) Casual blood glucose measurements in no
967 injection and injected mice (E9.5 injection and E10.5 injection). Each line represents an
968 individual mouse. No injection; WT, n = 3; *Pdx1*$^{+/-}$, n = 6; *Pdx1*$^{-/-}$, n = 3. Injected at E10.5; WT,
969 n = 4; *Pdx1*$^{+/-}$, n = 4; *Pdx1*$^{-/-}$, n = 3. Injected at E9.5; WT, n = 4; *Pdx1*$^{-/-}$, n = 6. (G) Human
970 C-peptide levels in serum of *Pdx1*$^{-/-}$ mice with or without injection at E9.5. ELISA
971 quantification comparing uninjected controls, injected mice at P0, and injected mice at P2.
972 Data shown as individual points with mean ± SEM. Statistical analysis by one-way ANOVA
973 with Tukey's post-hoc test, *$p < 0.05$. No injection n = 8, Injected (P0) n = 6, and Injected
974 (P2) n = 9. Experiments were done with EEF1A-iRFP670 line.
975
976 Figure 3 Human pancreatic cells engraft ectopically in the duodenum and undergo
977 pancreatic differentiation. (A) Experimental workflow showing intraplacental injection at E9.5
978 followed by chimerism analysis using ddPCR and FACS at P0. (B) Quantification of human
979 DNA distribution in various tissue by ddPCR. Percentage of human DNA detected in
980 different tissues from injected *Pdx1*$^{-/-}$ P0 newborns. n = 8 for all tissue, data shown as
981 individual points with mean ± SEM. Statistical analysis by one-way ANOVA with Tukey's
982 post-hoc test, *$p < 0.05$. (C) Flow cytometric detection of human cells in duodenum of *Pdx1*$^{-/-}$
983 at P0. Representative FACS plots showing iRFP/HLA double-positive populations in
984 uninjected versus injected *Pdx1*$^{-/-}$ duodenum samples. Quantification shows the percentage
985 of iRFP/HLA double-positive cells per DAPI-negative (live) cells. Data are shown as
986 individual sample and mean ± SEM. No injection, n = 5, injected, n = 10. Statistical analysis
987 by Welch's t-test, *$p < 0.05$. (D) Experimental workflow showing RNA-seq analysis from
988 sorted HLA/iRFP+ human cells. (E) PCA of transcriptomes from pancreatic progenitor cells
989 (PP; purple, n = 4) and sorted engrafted cells (Sorted; orange, n = 3) showing clear
990 separation. (F) Volcano plot of expressed genes between Sorted and PP populations.
991 Upregulated (orange) and downregulated (purple) genes are indicated ($|\log2 \text{ fold change}| >$
992 1, adjusted $p < 0.05$; DESeq2 Wald test). (G) Heatmap showing pancreatic progenitor
993 markers. (H) Heatmap showing upregulation of β-cell transcription factors and functional
994 genes in Sorted cells. (I) Heatmap of α-cell (GCG, ARX), ε-cell (GHRL) and δ-cell (SST)
995 marker expressions. (J) Heatmap of pancreatic exocrine marker expression. (K) Dot plots
996 comparing VST-normalized expression levels for key pancreatic genes between PP and

997 Sorted cells. Data are individual points with mean; n = 4 (PP) and n = 3 (Sorted); DESeq2
998 Wald test, p-values indicated. Experiments were done with EEF1A-iRFP670 line.
999
1000 Figure 4 Immunohistochemical confirmation of insulin-positive human cells in the duodenum.
1001 (A) Experimental workflow for immunohistochemical analysis. Schematic showing
1002 intraplacental injection of human pancreatic progenitors into *Pdx1*$^{+/-}$ × *Pdx1*$^{+/-}$ matings at
1003 E9.5, followed by collection of duodenal tissue from *Pdx1*$^{-/-}$ newborns at P0 for
1004 immunohistochemical analysis. (B) Representative immunofluorescence images of duodenal
1005 sections from three independent injected *Pdx1*$^{-/-}$ newborns at P0. Insulin (green) with DAPI
1006 (blue) showing insulin-positive cells integrated within duodenal villi. Left panels show low
1007 magnification overview with boxed regions, right panels show higher magnification of
1008 numbered regions (1, 2) containing insulin-expressing cells. Scale bar = 100 μm. (C) Control
1009 duodenal section from an uninjected *Pdx1*$^{-/-}$ newborn showing no detectable insulin-positive
1010 cells. Layout as in (B). (D) Quantification of insulin-positive cells as a percentage of total
1011 DAPI-positive cells per field. Eight fields were analyzed per sample. Data are shown as
1012 individual values with mean; Mann–Whitney U test, *$p < 0.05$. Experiments were done with
1013 EEF1A-iRFP670 line.
1014

Figure 1

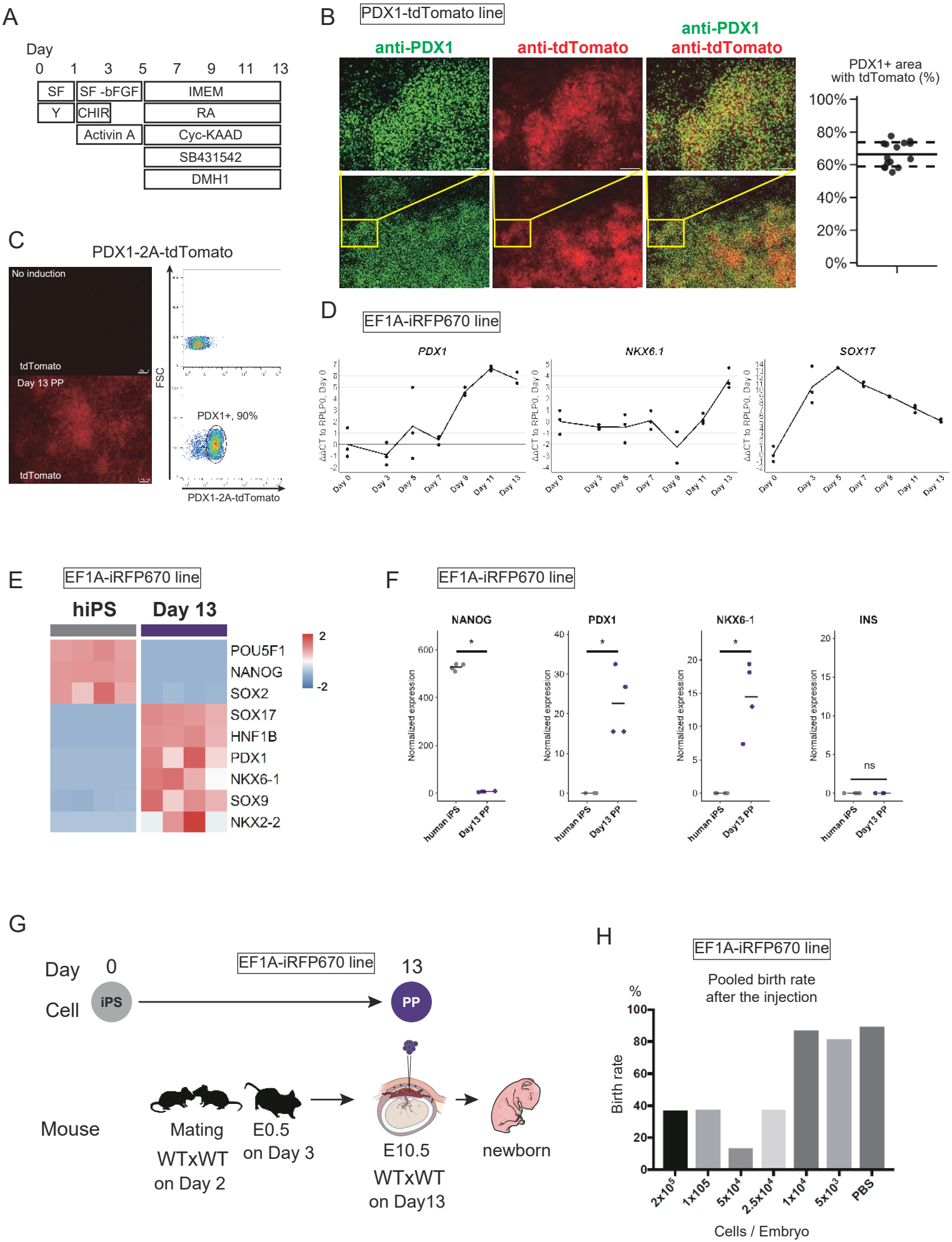
A
Day
0 1 3 5 7 9 11 13
SF
SF -bFGF
IMEM
Y
CHIR
RA
Activin A
Cyc-KAAD
SB431542
DMH1
B
PDX1-tdTomato line
anti-PDX1
anti-tdTomato
anti-PDX1
anti-tdTomato
PDX1+ area
with tdTomato (%)
100%
80%
60%
40%
20%
0%
C
PDX1-2A-tdTomato
No induction
tdTomato
Day 13 PP
tdTomato
FSC
PDX1+, 90%
PDX1-2A-tdTomato
D
EF1A-iRFP670 line
PDX1
NKX6.1
SOX17
ΔΔCT to RPLP0, Day 0
Day 0
Day 3
Day 5
Day 7
Day 9
Day 11
Day 13
E
EF1A-iRFP670 line
hiPS
Day 13
POU5F1
NANOG
SOX2
SOX17
HNF1B
PDX1
NKX6-1
SOX9
NKX2-2
2
-2
F
EF1A-iRFP670 line
NANOG
PDX1
NKX6-1
INS
Normalized expression
human iPS
Day13 PP
ns
G
Day
0
13
Cell
iPS
PP
EF1A-iRFP670 line
Mouse
Mating
WTxWT
on Day 2
E0.5
on Day 3
E10.5
WTxWT
on Day13
newborn
H
EF1A-iRFP670 line
Pooled birth rate
after the injection
%
Birth rate
2x10^5
1x10^5
5x10^4
2.5x10^4
1x10^4
5x10^3
PBS
Cells / Embryo

Figure 2

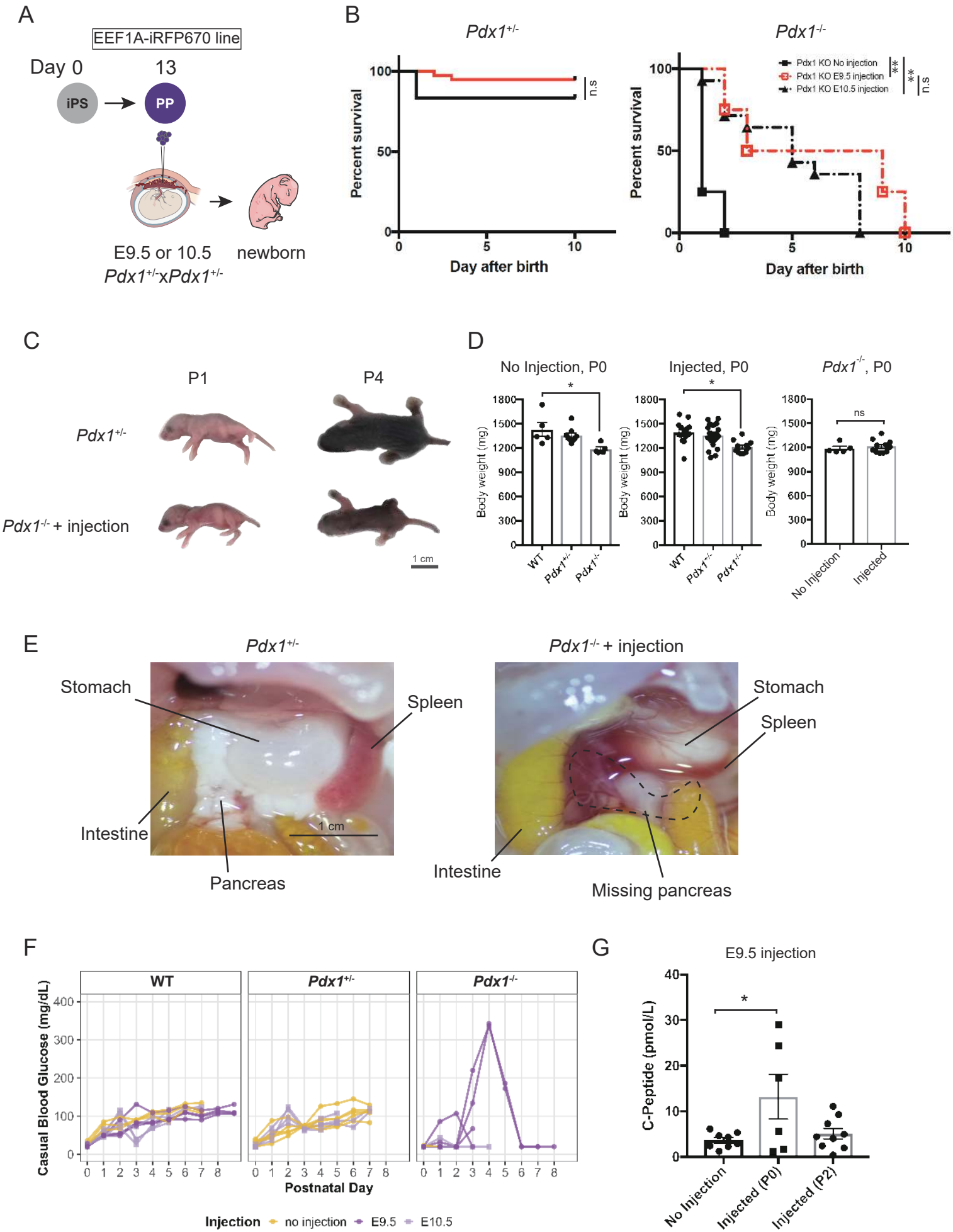
A
EEF1A-iRFP670 line
Day 0
13
iPS
PP
E9.5 or 10.5
Pdx1+/-xPdx1+/-
newborn
B
Pdx1+/-
Pdx1-/-
Percent survival
Day after birth
n.s
Pdx1 KO No injection
Pdx1 KO E9.5 injection
Pdx1 KO E10.5 injection
**
C
P1
P4
Pdx1+/-
Pdx1-/- + injection
1 cm
D
No Injection, P0
Injected, P0
Pdx1-/-, P0
Body weight (mg)
WT
Pdx1+/-
Pdx1-/-
No Injection
Injected
ns
E
Pdx1+/-
Pdx1-/- + injection
Stomach
Spleen
Intestine
Pancreas
1 cm
Missing pancreas
F
WT
Casual Blood Glucose (mg/dL)
Postnatal Day
Injection
no injection
E9.5
E10.5
G
E9.5 injection
C-Peptide (pmol/L)
No Injection
Injected (P0)
Injected (P2)

Figure 3

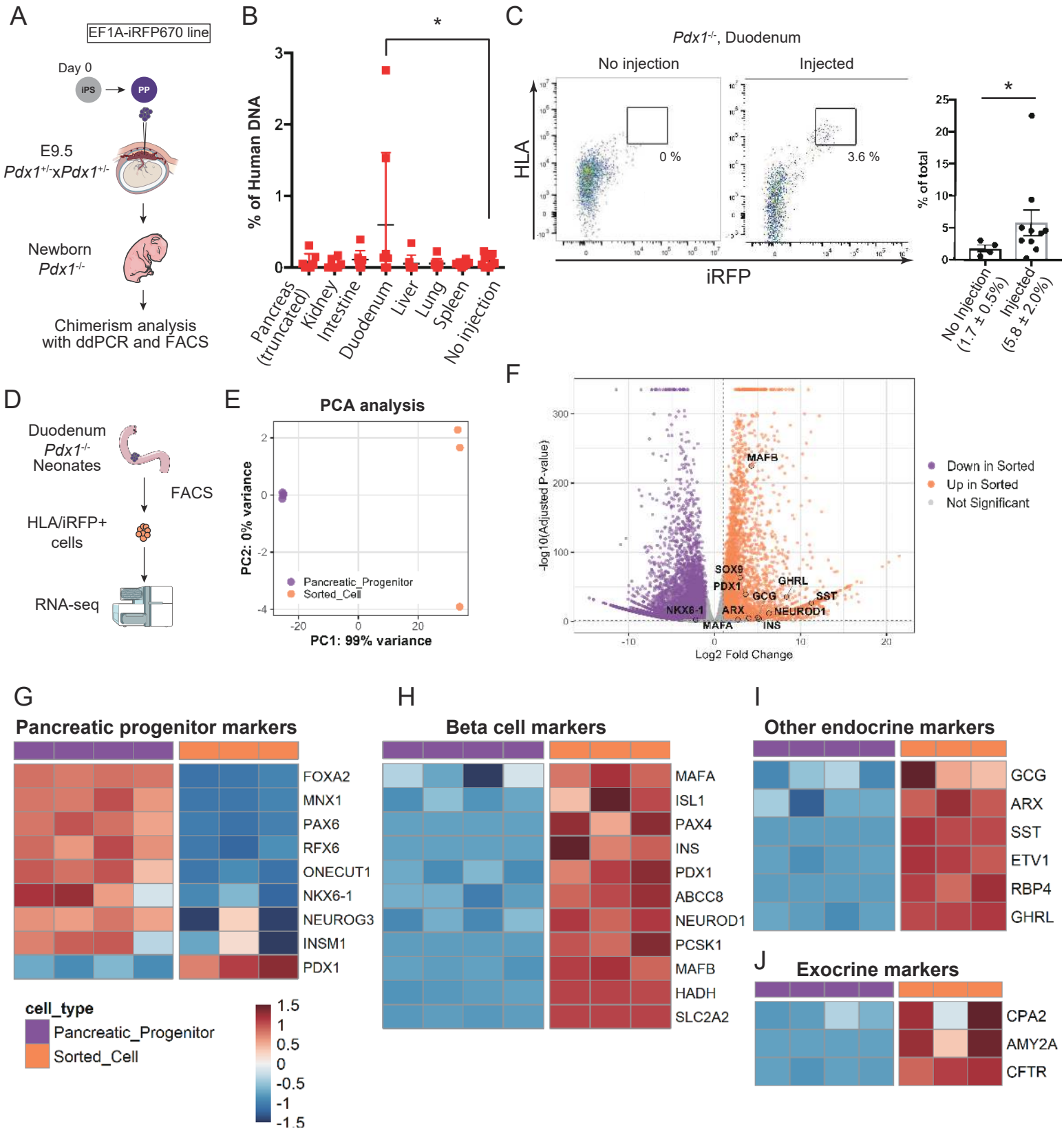
A
EF1A-iRFP670 line
Day 0
iPS
PP
E9.5
Pdx1+/-xPdx1+/-
Newborn
Pdx1-/-
Chimerism analysis
with ddPCR and FACS
B
% of Human DNA
Pancreas (truncated)
Kidney
Intestine
Duodenum
Liver
Lung
Spleen
No injection
C
Pdx1-/-, Duodenum
No injection
Injected
HLA
iRFP
0 %
3.6 %
% of total
No Injection (1.7 ± 0.5%)
Injected (5.8 ± 2.0%)
D
Duodenum
Pdx1-/-
Neonates
FACS
HLA/iRFP+
cells
RNA-seq
E
PCA analysis
PC2: 0% variance
PC1: 99% variance
Pancreatic_Progenitor
Sorted_Cell
F
-log10(Adjusted P-value)
Log2 Fold Change
MAFB
SOX9
PDX1
GHRL
GCG
SST
NKX6-1
ARX
NEUROD1
MAFA
INS
Down in Sorted
Up in Sorted
Not Significant
G
Pancreatic progenitor markers
FOXA2
MNX1
PAX6
RFX6
ONECUT1
NKX6-1
NEUROG3
INSM1
PDX1
cell_type
Pancreatic_Progenitor
Sorted_Cell
H
Beta cell markers
MAFA
ISL1
PAX4
INS
PDX1
ABCC8
NEUROD1
PCSK1
MAFB
HADH
SLC2A2
I
Other endocrine markers
GCG
ARX
SST
ETV1
RBP4
GHRL
J
Exocrine markers
CPA2
AMY2A
CFTR
K
NKX6-1
Log2FC = -2.21, p-adj = 6.50e-03
NEUROD1
Log2FC = 6.33, p-adj = 2.98e-12
INS
Log2FC = 5.16, p-adj = 4.17e-04
GCG
Log2FC = 5.02, p-adj = 3.22e-06
SST
Log2FC = 11.25, p-adj = 3.15e-27
Log2-transformed expression
PP
Sorted

Figure 4

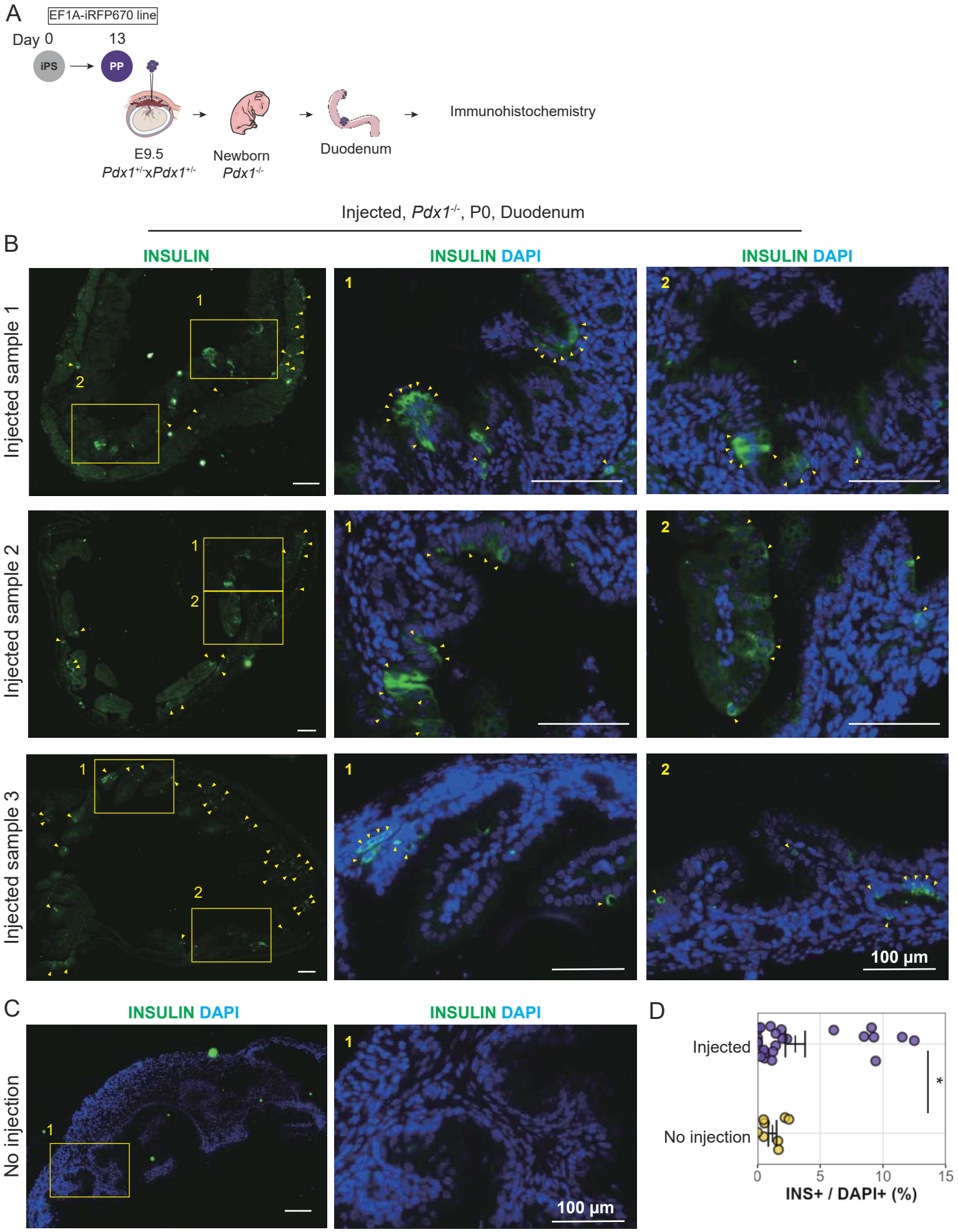
A
EF1A-iRFP670 line
Day 0
13
iPS
PP
E9.5
Pdx1+/-xPdx1+/-
Newborn
Pdx1-/-
Duodenum
Immunohistochemistry
Injected, Pdx1-/-, P0, Duodenum
B
INSULIN
INSULIN DAPI
INSULIN DAPI
Injected sample 1
Injected sample 2
Injected sample 3
1
2
100 µm
C
INSULIN DAPI
INSULIN DAPI
No injection
100 µm
D
Injected
No injection
0
5
10
15
INS+ / DAPI+ (%)
*